BRAIN
ORIGINAL ARTICLE

# Frontostriatothalamic effective connectivity and dopaminergic function in the psychosis continuum

Kristina Sabaroedin,[1] Adeel Razi,[1,2,3] Sidhant Chopra,[1] Nancy Tran,[1] Andrii Pozaruk,[2] Zhaolin Chen,[2] Amy Finlay,[1] Barnaby Nelson,[4,5] Kelly Allott,[4,5] Mario Alvarez-Jimenez,[4,5] Jessica Graham,[4,5] Hok P. Yuen,[4,5] Susy Harrigan,[6,7] Vanessa Cropley,[8] Sujit Sharma,[9] Bharat Saluja,[9] Rob Williams,[10] Christos Pantelis,[8,11] Stephen J. Wood,[4,5,12] Brian O'Donoghue,[4,5] Shona Francey,[4,5] Patrick McGorry,[4,5] Kevin Aquino[1,2] and Alex Fornito[1,2]

Dysfunction of fronto-striato-thalamic (FST) circuits is thought to contribute to dopaminergic dysfunction and symptom onset in psychosis, but it remains unclear whether this dysfunction is driven by aberrant bottom-up subcortical signalling or impaired top-down cortical regulation.

We used spectral dynamic causal modelling of resting-state functional MRI to characterize the effective connectivity of dorsal and ventral FST circuits in a sample of 46 antipsychotic-naïve first-episode psychosis patients and 23 controls and an independent sample of 36 patients with established schizophrenia and 100 controls. We also investigated the association between FST effective connectivity and striatal $^{18}$F-DOPA uptake in an independent healthy cohort of 33 individuals who underwent concurrent functional MRI and PET.

Using a posterior probability threshold of 0.95, we found that midbrain and thalamic connectivity were implicated as dysfunctional across both patient groups. Dysconnectivity in first-episode psychosis patients was mainly restricted to the subcortex, with positive symptom severity being associated with midbrain connectivity. Dysconnectivity between the cortex and subcortical systems was only apparent in established schizophrenia patients. In the healthy $^{18}$F-DOPA cohort, we found that striatal dopamine synthesis capacity was associated with the effective connectivity of nigrostriatal and striatothalamic pathways, implicating similar circuits to those associated with psychotic symptom severity in patients. Overall, our findings indicate that subcortical dysconnectivity is evident in the early stages of psychosis, that cortical dysfunction may emerge later in the illness, and that nigrostriatal and striatothalamic signalling are closely related to striatal dopamine synthesis capacity, which is a robust marker for psychosis.

1 Turner Institute for Brain and Mental Health, School of Psychological Sciences, Monash University, Clayton, Victoria 3800, Australia
2 Monash Biomedical Imaging, Monash University, Clayton, Victoria 3800, Australia
3 Wellcome Centre for Human Neuroimaging, University College, London WC1N 3AR, UK
4 Orygen, Parkville, Victoria 3052, Australia
5 Centre for Youth Mental Health, The University of Melbourne, Parkville, Victoria 3052, Australia
6 Department of Social Work, Monash University, Victoria 3800, Australia
7 Melbourne School of Population and Global Health, The University of Melbourne, Parkville. Victoria 3010, Australia
8 Melbourne Neuropsychiatry Centre, Department of Psychiatry, The University of Melbourne & Melbourne Health, Parkville, Victoria 3010, Australia
9 Monash Health, Dandenong, Victoria 3175, Australia

Received July 28, 2021. Revised December 21, 2021. Accepted December 22, 2021. Advance access publication January 30, 2022

10 The University of Melbourne, Parkville, Victoria 3010, Australia
11 The Florey Institute for Neuroscience and Mental Health, The University of Melbourne, Parkville, Victoria 3052, Australia
12 School of Psychology, University of Birmingham, Edgbaston, Birmingham B15 2TT, UK

Correspondence to: Kristina Sabaroedin
Turner Institute for Brain and Mental Health
770 Blackburn Road, Clayton, Victoria 3168, Australia
E-mail: Kristina.Sabaroedin@monash.edu

Keywords: effective connectivity; dopamine; frontostriatal; psychosis; schizophrenia

## Introduction

Dysfunction of fronto-striato-thalamic (FST) circuits linking the caudate and putamen with the prefrontal cortex is thought to be central to the emergence of psychotic symptoms.[1–6] Two such circuits are particularly relevant: (i) a ventral 'limbic' system involved in emotional and reward processing, which connects the orbital and ventromedial prefrontal cortices and subcortical limbic structures (e.g. hippocampus and amygdala) with the nucleus accumbens (NAcc); and (ii) a dorsal 'associative' system, which links the dorsolateral prefrontal cortex (dlPFC) with the dorsal striatum, and subserves associative learning and executive functions.[1,7] Feedback loops passing through the pallidum and the thalamus connect both circuits back to the cortex.[1]

The striatum is a major target for dopamine projections from the ventral tegmental area (VTA) and substantia nigra (SN), with the ventral and the dorsal regions respectively forming part of the mesolimbic and nigrostriatal pathways.[8] Dysregulated dopamine signalling is proposed to contribute to psychosis onset by influencing the capacity of the striatum to filter and relay information to the thalamus, thus affecting broader FST function.[9] *In vivo* PET has revealed elevated presynaptic dopamine synthesis capacity, measured using 3,4-dihydroxy-6-$^{18}$F-fluoro-L-phenylalanine ($^{18}$F-DOPA), in the dorsal striatum of at-risk groups, especially in individuals who transition to psychosis.[10,11] Increased dopamine binding and release in the dorsal striatum have also been shown in psychosis patients and at-risk individuals.[12,13] Moreover, $^{18}$F-DOPA elevations in the ventral striatum of schizophrenia patients and of at-risk individuals have been reported.[14,15] In parallel, resting-state functional MRI (fMRI) studies have identified reduced functional connectivity between the dorsal striatum, thalamus, and dlPFC in first episode psychosis (FEP) patients, their unaffected first-degree relatives, at-risk individuals, chronic unmedicated patients, and healthy people with psychosis-like experiences.[2–5,16,17] Increased functional connectivity between the ventral striatum, limbic regions, anterior cingulate cortex, ventromedial prefrontal and orbitofrontal cortices has also been found in these groups.[2,18–20] Correlations between striatal $^{18}$F-DOPA activation of prefrontal and medial temporal areas have been reported in early and chronic stages of psychotic illness.[21–23]

Functional connectivity quantifies statistical dependencies between regional activity and does not distinguish causal interactions. It is therefore unclear whether FST dysfunction in psychosis arises from altered bottom-up signalling or disrupted top-down regulation of subcortical systems. Evidence for a primary bottom-up pathology comes from reports of aberrant molecular function, activity, and functional connectivity of the midbrain across at-risk and schizophrenia groups.[24–26] Others have proposed, largely based on *ex vivo* and preclinical findings, that subcortical changes are secondary to deficient top-down control of midbrain neurons, which is caused by GABA/glutamate imbalance in the cortex or hippocampus.[9,27,28] However, *in vivo* imaging findings have been mixed, with reports of increased, decreased, or no changes in prefrontal excitatory or inhibitory metabolites in FEP[29–33] and people with established schizophrenia (SCZ).[30,31,34,35]

Top-down and bottom-up interactions between distinct elements of FST systems can be disentangled through models of effective connectivity. Effective connectivity refers to the causal influence that one neural system exerts over another,[36] which can be estimated from fMRI data using dynamic causal modelling (DCM). DCM uses a Bayesian framework for optimizing a generative model of directed, or causal, influences between regions comprising a distributed neural system.[36] In DCM, inter-regional connections are referred to as extrinsic connections,[37] and they can be used to infer top-down influences from cortical to subcortical areas or bottom-up subcortical-to-cortical interactions. Another important feature of DCM is that it allows the investigation of the intrinsic functioning of a brain region through the estimation of recurrent inhibition, modelled as a self-connection, which can uncover intra-regional pathology.[37] Here, we used spectral DCM[38] of resting-state fMRI data to characterize disruptions of extrinsic and recurrent intrinsic effective connectivity within dorsal and ventral FST systems in antipsychotic-naïve FEP patients and people with SCZ, as well as associations with psychotic symptoms, which have historically been linked to FST dysfunction.[39] In an independent healthy cohort who underwent concurrent fMRI and $^{18}$F-DOPA PET, we then identified the specific FST connections that are associated with dorsal and ventral striatal $^{18}$F-DOPA levels. This approach allowed us to cross-sectionally map effective dysconnectivity of FST circuits across different illness stages and to identify putative directed influences associated with striatal dopamine synthesis capacity, a robust marker of illness risk.[10,40,41]

## Materials and methods

### Participants

We examined three independent cohorts: (i) an FEP cohort comprising antipsychotic-naïve patients within 6 months of psychosis onset and healthy controls[42]; (ii) a SCZ cohort comprising schizophrenia patients and healthy controls obtained through the

UCLA Consortium for Neuropsychiatric Phenomics open dataset[43]; and (iii) an $^{18}$F-DOPA cohort comprising healthy participants recruited from the community who underwent concurrent PET/fMRI scans. The FEP and SCZ cohorts allowed us to examine FST effective connectivity at distinct illness stages, while the $^{18}$F-DOPA cohort allowed us to identify specific connections associated with striatal dopamine synthesis capacity. Separate analyses were also performed for a subgroup of the FEP cohort with a schizophrenia diagnosis (FEP-SCZ) to examine whether there were diagnosis-specific effects within the FEP group. Group numbers and demographic details are provided in Table 1. The recruitment of our FEP cohort, controls, and the $^{18}$F-DOPA cohort was in accordance with the Melbourne Health Human Research Ethics Committee (reference numbers 2007.616 and 1443066.1). Below are the recruitment details for each of our cohort. Detailed description of the number of recruited participants excluded from our analyses are outlined in the Supplementary material.

### First-episode psychosis

Participants were aged 15–25 years, presenting with FEP to an early psychosis intervention centre at Orygen Youth Health, Melbourne, Australia.[42] FEP was defined as fulfilling Structured Clinical Interview for DSM-5 (SCID-5) criteria for a psychotic disorder. Patients with substance-induced psychosis were excluded in the present study. Healthy controls had no history of psychiatric or neurological illness, as determined by self-reports, SCID, and the Comprehensive Assessment of At-Risk Mental States. Recruitment occurred from April 2008 to December 2016. All participants provided informed consent. For FEP patients, additional strict inclusion criteria included comprehension of English language, no contraindication to MRI scanning, less than 6 months duration of untreated psychosis, living in stable accommodation, low risk to self or others [score of <5 on the Brief Psychiatric Rating Scale version 4 (BPRS-4) Suicidality and Hostility subscales], and minimal previous exposure to antipsychotic medication (less than 7 days of use or lifetime 1750 mg chlorpromazine equivalent exposure). Healthy controls were age-matched to patients. Additional exclusion criteria for controls included history of psychiatric or neurological illness in first-degree relatives and current use of psychotropic medications. A total of 46 patients and 23 controls were included in our final analyses. We also analysed a subsample of the FEP-SCZ cohort ($n = 17$) to identify the differences in connectivity based on differential diagnoses.

### Established schizophrenia

Data were obtained through the UCLA Consortium for Neuropsychiatric Phenomics (CNP) open dataset.[43] The initial sample consisted of 121 right-handed healthy controls and 51 patients with SCZ aged between 21–50 years old. Healthy controls were excluded if they had a lifetime history of mental illness, including SCZ or other psychotic disorders, and bipolar disorders. Healthy controls were also excluded on current diagnosis of major depressive disorder, suicidality, anxiety disorder, or attention deficit hyperactivity disorder (ADHD). Additional exclusion criteria for all participants included left-handedness, pregnancy, neurological disease, history of head injury with loss of consciousness or cognitive sequelae, use of psychoactive medications, substance abuse or dependence, and other MRI contraindications (e.g. claustrophobia). SCZ patients were also excluded if they had comorbidity with either bipolar disorder or ADHD. Diagnoses were based on the DSM-IV and SCID-1. All SCZ patients were on stable medication. Mean lifetime chlorpromazine-equivalent dose[44] for patients with available medication information is 662.51 mg (SD = 764.91 mg; $n = 28$). No significant correlations between antipsychotic exposure and effective connectivity were identified (i.e. all $P > 0.05$, corrected). A total of 36 patients and 100 controls were included in our analyses after quality checking.

### Healthy $^{18}$F-DOPA cohort

A total of 52 healthy participants aged 18–28 years were recruited from the community through online advertisements. Recruitment period was between May 2016 until May 2019. Each participant provided informed consent. Exclusion criteria included current or history of psychiatric or neurological illnesses, significant medical history, intellectual disability, and first-degree relative with a mental illness. Participants underwent simultaneous resting-state fMRI and PET imaging with $^{18}$F-DOPA tracer. A total of 33 participants were included in our final analyses.

## Symptom measures

Positive symptoms were assessed in patients using the positive subscale of Brief Psychiatric Rating Scale (BPRS) version 4.[45] The subscales were derived from a five factor solution outlined in Dazzi *et al.*[45] Psychotic symptom scores were derived from the positive symptom subscale which consists of five items: unusual

**Table 1 Descriptive statistics of participants**

| | FEP | | | SCZ | | $^{18}$F-DOPA |
|---|---|---|---|---|---|---|
| | HC ($n = 23$) | FEP ($n = 46$) | FEP-SCZ ($n = 17$) | HC ($n = 100$) | SCZ ($n = 36$) | HC ($n = 33$) |
| Males, *n* (%) | 14 (60.87) | 20 (43.48) | 9 (41.18) | 55 (55) | 26 (72.22) | 15 (45.45) |
| Age, mean (SD) | 21.74 (1.92) | 19.12 (2.97) | 20.51 (2.87) | 30.6 (8.87) | 35.81(8.49) | 22.30 (2.21) |
| Age range, years | 18–26 | 15–25 | 15–25 | 21–50 | 22–49 | 18–28 |
| **BPRS total** | | | | | | |
| Mean (SD) | — | 56.91 (10.34) | 61.94 (9.41) | — | 49.39 (14.03) | — |
| Range | — | 38–80 | 46–80 | — | 26–77 | — |
| **BPRS positive** | | | | | | |
| Mean (SD) | — | 15.65 (4.19) | 17.94 (4.31) | — | 14.11 (6.17) | — |
| Range | — | 10–27 | 13–27 | — | 5–29 | — |
| **BPRS negative** | | | | | | |
| Mean (SD) | — | 5.76 (2.6) | 7 (3.16) | — | 5.14 (2.54) | — |
| Range | — | 3–12 | 3–12 | — | 3–11 | — |

$^{18}$F-DOPA = healthy group who underwent a simultaneous PET-fMRI protocol; HC = healthy controls.

thought content, suspiciousness, hallucinations, grandiosity, and bizarre behaviour. Secondary analyses also considered negative symptoms assessed with the same instrument. The negative symptom subscale consists of three items: blunted affect, emotional withdrawal, and motor retardation. Each item is ranked on a Likert-like scale between 1 to 7, with a score of 1 denoting the absence of a measured symptom.

## Functional MRI acquisition

The scanning acquisition protocol for each participant group is described as follows.

### First-episode psychosis

Whole-brain $T_2^*$-weighted echo-planar images (EPIs) and anatomical $T_1$-weighted scans were acquired for each participant using a 3 T Siemens Trio Tim scanner, equipped with a 32-channel head coil, located at the Royal Children's Hospital in Melbourne, Australia. Participants were instructed to lie still in the scanner while maintaining wakefulness with eyes closed. A total of 234 functional volumes with 37 slices each were acquired using the following parameters: repetition time (TR) = 2000 ms; echo time (TE) = 32 ms; flip angle = 90°; field of view (FOV) = 210 mm; slice thickness of 3.5 mm; and 3.3 × 3.3 × 3.55 mm voxels. A total of 176 slices were acquired for each participant's $T_1$-weighted image using an interleaved acquisition using the following parameters: TR = 2.3 s; TE = 2.98 ms; flip angle of 9°; FOV of 256 mm; voxel size of 1.1 × 1.1 × 1.2 mm.

### Established schizophrenia

The UCLA CNP dataset[43] was acquired on one of two Siemens Trio 3 T scanners located at the Ahmanson-Lovelace Brain Mapping Center and the Staglin Center for Cognitive Neuroscience at UCLA. Details of the resting-state EPI scan were TR = 2 s, TE = 30 ms, flip angle = 90°, 4 mm slice thickness, 152 volumes, with 34 slices each. Participants were instructed to keep their eyes open. Details of the $T_1$-weighted scan were TR = 1.9 s, TE = 2.26 ms, flip angle of 90°, 176 slices, with 1 $mm^3$ voxels.

### $^{18}$F-DOPA

Data were acquired using a 3 T Siemens Magnetom Biograph simultaneous MR-PET scanner equipped with a 20-channel head and neck coil at Monash Biomedical Imaging, Melbourne, Australia. Resting-state whole-brain $T_2^*$-weighed EPIs were also acquired for each subject using an interleaved acquisition with the following parameters: TR = 2.89 s; TE = 30 ms; 152 volumes, with 44 slices per volume; flip angle = 90°; FOV = 190 mm; slice thickness = 3 mm; voxel size of 3 $mm^3$. A high resolution $T_1$-weighted anatomical image was acquired for each subject using an ascending acquisition (176 slices; TR = 1640 ms; TE = 2.34 ms; flip angle = 8°; FOV = 256 mm; slice thickness = 1 mm; voxel size = 1 $mm^3$).

## MRI processing

Functional MRI and $T_1$-weighted data were processed in the same way across all three cohorts using FMRIPREP software version 1.1.1.[46] Each $T_1$-weighted scan was corrected for non-uniformity in intensity and subsequently skull stripped. Brain surfaces were reconstructed using FreeSurfer version 6.0.1. Tissue masks were generated using FreeSurfer. Spatial normalization of the skull stripped $T_1$-weighted images to the ICBM 152 Nonlinear Asymmetrical template version 2009c was performed using a nonlinear registration in Advanced Normalization Tools (ANTs) version 2.1.0. Similarly, for each participant, tissue masks were registered from the surface space to the Montreal Neurological Institute (MNI) template.

EPIs were slice-timed corrected using AFNI version 16.2.07 and realigned to a mean reference image using FSL. EPIs were distortion corrected using fieldmaps (phasediff-based workflow; https://fmriprep.readthedocs.io/en/stable/api/index.html#sdc-phasediff). For participants with missing fieldmaps, a 'fieldmap-less' distortion correction was performed by co-registering the functional image to the intensity-inverted $T_1$-weighted image constrained with an EPI distortion atlas.[47] Following distortion correction, EPIs were co-registered with their corresponding $T_1$-weighted image using boundary-based registration with nine degrees of freedom using the bbregister routine in FreeSurfer. The motion-correcting transformations, field-distortion-correcting warp, EPI-to-$T_1$-weighted transformation, and $T_1$-weighted-to-MNI template warp were concatenated and applied in a single step using ANTs version 2.1.0. In-scanner head motion was defined as excessive according to previously-defined stringent exclusion criteria;[48] namely, if any of the following were met: (i) mean framewise displacement (FD) > 0.20 mm; (ii) sum of suprathreshold FD spikes > 20%; and (iii) any FD > 5 mm. FD was calculated using the root mean squared volume-to-volume displacement of all voxels, derived from the six head motion parameter (three translations, three rotations).[48] ICA-based Automatic Removal of Motion Artifacts (AROMA) was used to generate noise regressors.[49] ICA-AROMA noise components were non-aggressively regressed out from the EPI data. Next, white matter and CSF signals were estimated from each subject using restricted tissue masks and were removed out from the data via linear regression. A high-pass filter of 200 s was the applied to each EPI image prior to spatial smoothing using a Gaussian kernel of 4 mm full-width half-maximum implemented using the 3dBlurToFWHM function in AFNI (version 16.2.16). We did not perform global signal regression as DCM incorporates noise parameter estimates that capture observation noise due to scanner and physiological noise[38,50] and also because it may remove real neuromodulatory fluctuations in neuronal activity, which are of key interest in the present study (for a discussion, see Aquino *et al.*[51] and Glasser *et al.*[52]).

## PET acquisition, processing and analysis

PET data in the $^{18}$F-DOPA group were acquired on a MR-PET Siemens Biograph scanner. All participants received carbidopa (150 mg) and entacapone (400 mg) orally 60 min before imaging to reduce the formation of radiolabeled metabolites that can cross the blood–brain barrier and thus confound tracer availability in the striatum.[53,54] All subjects were administered approximately 150 Mbq of $^{18}$F-DOPA via interbolus injection at the start of the PET imaging. Participants were instructed to lie still in the scanner with eyes closed. Participants were instructed to lie still in the scanner with eyes closed.

The pseudo-CT attenuation correction method[55,56] was used to correct PET images during image reconstruction. Dynamic PET images were reconstructed using the Siemens e7tools software with image volume size 344 × 344 × 127 (2.09 × 2.09 × 2.03 $mm^3$). The Ordinary Poisson-Ordered Subset Expectation Maximization (OP-OSEM) algorithm (three iterations, 21 subsets) was used with the point spread function (PSF) for partial volume correction. A 5-mm full-width at half-maximum Gaussian filter was applied to

each 3D image volume. For correction of subject motion, the list mode dataset was first binned into 95 frames consisting of one 30-s background frame and ninety-four 60-s frames. Dynamic motion was corrected based on an image registration approach,[57] where each frame was registered to the last frame using rigid-body transformation implemented in the FSL toolbox.[58] The final reconstructed dynamic PET images were registered to the corresponding $T_1$ Magnetization-Prepared Rapid Gradient-Echo Imaging MRI image. Patlak graphical analysis[59] was performed using Qmodeling software[60] to quantify $^{18}$F-DOPA influx rate constants ($K_i^{cer}$ values) for dorsal and ventral striatal regions of interest (ROIs)[61] (Supplementary Fig. 1) relative to the cerebellum[62] in each participant's anatomical space. We only analysed the left hemisphere consistent with our DCM (see below).

## Dynamic causal modelling

### Model space selection

ROIs spanning the dorsal and ventral FST systems, and the midbrain, were selected using stereotactic coordinates of past findings or of peak signals identified using functional connectivity. Effective connectivity explains the change of activity in one region as a function of activity in another region and does not depend on signal correlations between two areas. As such, selecting regions based on functional connectivity peaks does not result in biased ROI selection. We modelled 47 biologically plausible connections, identified through tract tracing or human functional connectivity, between eight ROIs (Fig. 1). The first eigenvariate of the time-series of each ROI was extracted and entered into a first-level DCM analysis. We focused on the left hemisphere given prior evidence of more consistent functional connectivity effects in left-lateralized FST circuits in patients.[2,3] Spherical ROIs were created with a radius of 6 mm for cortical regions [i.e. dlPFC and ventromedial PFC (vmPFC)] and 3.5 mm for each subcortical ROI. For vmPFC and thalamus ROIs with centroids that were close to the anatomical or functional boundary of the region, we used an anatomical mask from the FreeSurfer package when extracting the first eigenvariate for the ROIs to exclude signal from neighbouring regions. Details of the ROI selection for each region are provided below.

#### Nucleus accumbens and dorsal caudate

For the ventral and dorsal striatum, we seeded the NAcc and dorsal caudate (DC) consistent with our previous works[2,4,63] using a functional parcellation of the striatum[64] that was delineated based on a meta-analysis of striatal activation in fMRI and PET studies.[65] The pallidum, which is the primary output structure of the basal ganglia, was omitted to limit model dimensionality. Its effects will thus be captured through indirect (unmodelled) influences in the DCM.

#### Dorsolateral prefrontal cortex

To capture variations associated with risk for psychosis as well as disruptions in clinical groups, the dlPFC ROI was selected based on a peak in which functional connectivity with the DC was reduced in the healthy relatives of FEP patients compared to healthy controls.[2] This peak overlapped with an area that also showed reduced connectivity in patients.

#### Ventromedial prefrontal cortex

To choose a region that was most relevant to the ventral circuit, we chose a peak in the vmPFC that showed strong functional connectivity with the NAcc in an independent cohort of 353 healthy adults.[4]

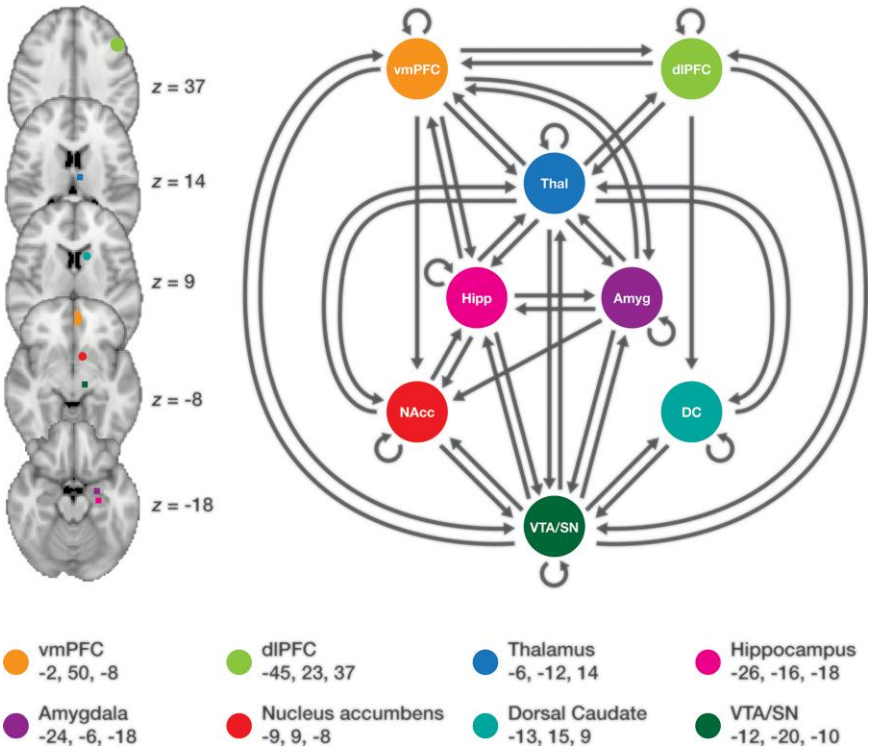


**Figure 1 Parent model space of FST systems encompassing dorsal and ventral circuits.** *Left*: Anatomical locations of ROIs on axial slices. *Right*: The parent model, including 47 biologically plausible connections including self-connections (circular arrows) for a network comprising eight regions. *Bottom*: Centroids of ROIs in MNI coordinates (x, y, z). Amyg = amygdala; Hipp = hippocampus; Thal = thalamus.

#### Thalamus

The thalamus coordinate was selected from a peak in which functional connectivity with the dorsal caudate was reduced in at-risk mental state individuals compared to healthy controls.[63]

#### Hippocampus and amygdala

ROIs for these regions were selected using a similar method. Peak coordinates within anatomical masks for the hippocampus and amygdala were selected in a separate group-level functional connectivity analysis of each ROI's connectivity with the whole brain in an independent cohort of 353 individuals.[4] For the hippocampus, we chose the anterior region, using of a hippocampal mask provided in the Freesurfer package.[66] The anterior hippocampus is a hippocampal region that is most frequently implicated as dysfunctional in schizophrenia,[67] and it was defined as the region having the MNI coordinate of less than $y = -22$.[68] Similar to the hippocampus, we used an amygdala mask provided in FreeSurfer.

#### Midbrain

The midbrain is a challenging area to identify due to the lack of tissue contrast afforded by anatomical $T_1$ scans. We therefore employed a midbrain mask derived from a comprehensive study of functional connectivity between the VTA, SN, and the rest of the brain, which has been that was validated in two independent datasets.[69] Due to the coarse resolution of the functional scans, we combined VTA and SN into one midbrain ROI, which limits our ability to delineate mesolimbic and nigrostriatal pathways. We selected a functional connectivity signal peak in the same cohort that was used in the selection of our hippocampal, amygdala, and vmPFC ROIs.

### Model estimation

We modelled effective connectivity in the spectral domain by fitting a complex cross spectral density using a generative model, parametrized by a power-law model of endogenous fluctuations, implemented in SPM12 (DCM 12; revision 7487).[38] Details are provided in the Supplementary material. Briefly, subject-specific first-level analyses were used to estimate directed (causal) influences between regions (in Hz), and the (inhibitory) recurrent or self-connectivity (i.e. self-inhibition) within each region.

Subject-specific connectivity parameters were then passed to a group-level general linear model (GLM) implemented in the parametric empirical Bayes (PEB) framework to estimate between-subject variability.[70] PEB models were run separately for each cohort. FEP and SCZ patients were compared to their respective control groups. Symptom associations in patients were modelled separately for each group for each connection in the model space, with both positive and negative symptoms included as covariates. Associations with $^{18}$F-DOPA were modelled in healthy individuals only, with dorsal and ventral striatal $K_i^{cer}$ values as covariates. Age, sex, and mean FD[71] were used as nuisance covariates for all models to address unequal distributions of sex across groups, as well as age and head motion as confounding variables. Scanner site was also used as a covariate in the SCZ group. We only report effects with a posterior probability threshold above 0.95. This threshold is based upon the differences in model evidence, or marginal likelihood, observed when comparing models with and without a particular connection. Critically, PEB is a multivariate (Bayesian) GLM in which we fit all model parameters at once; hence, no correction for multiple comparisons is required. A typical effect size for effective connectivity between regions is 0.1 Hz.[38] Self-connections are inhibitory to reflect activity decay, with a negative sign indicating reduced self-inhibition (i.e. disinhibition, or slower activity decay) and a positive sign indicating increased self-inhibition (i.e. quicker activity decay). Note that a group difference of 0 Hz in effective connectivity does not imply the absence of that connection in either group, but instead signifies that the groups do not differ in their effective connectivity. A mean connectivity of 0 Hz within a group denotes an absence of effective connectivity, but it does not necessarily imply a lack of anatomical connectivity. Technical details are outlined in the Supplementary material.

### Checks on variance explained

Connectivity methods based on correlations such as functional connectivity depend on covariances between brain regions, which are influenced by observation noise and changes in signal-to-noise ratio.[37] In contrast to descriptive correlational methods, DCM accounts for noise by modelling observation noise in the data, which includes thermal and physiological noise[50] (see Equations 2 and 3 in Supplementary material). The DCM routine also incorporates a diagnostic check to determine the accuracy of model inversion by calculating the percentage of variance explained by the model based on the predicted brain oxygen level-dependent signal.[72] Based on this diagnostic check, we excluded subjects with <75% variance explained by DCM for subsequent analyses following first-level model inversion (details in Supplementary material).

### Data availability

Data from the UCLA Consortium for Neuropsychiatric Phenomics are available on an open dataset platform on https://openneuro.org/datasets/ds000030/versions/00016. Derived data from our FEP and PET cohorts are available from the corresponding author on request.

## Results

### Group differences in effective connectivity

#### First-episode psychosis patients versus healthy controls

To examine FST disruptions at the earliest signs of illness, before exposure to antipsychotic medication, we first investigated effective connectivity disruptions in antipsychotic-naive FEP patients relative to healthy controls. Patients showed reduced self-inhibition of VTA/SN, increased self-inhibition of dlPFC, greater inhibitory influence of the thalamus on NAcc, and a greater excitatory influence of the amygdala on NAcc (Fig. 2A and Table 2). The subset of FEP-SCZ patients (Fig. 2B and Table 2) showed similar changes but did not show increased dlPFC self-inhibition. FEP-SCZ patients additionally demonstrated a relative disinhibition of the amygdala, increased excitatory influence of VTA/SN on NAcc, and increased inhibitory influence of VTA/SN and NAcc on hippocampus. Connections between cortical and subcortical ROIs were not implicated as dysfunctional in FEP patients.

#### Patients with established schizophrenia versus healthy controls

We next examined, in an independent sample of patients and controls, whether people with SCZ show similar disruptions of FST effective connectivity to those observed in FEP. As with FEP, we found that SCZ patients showed disinhibition of VTA/SN and a greater inhibitory influence of thalamus on NAcc relative to controls (Fig. 2C

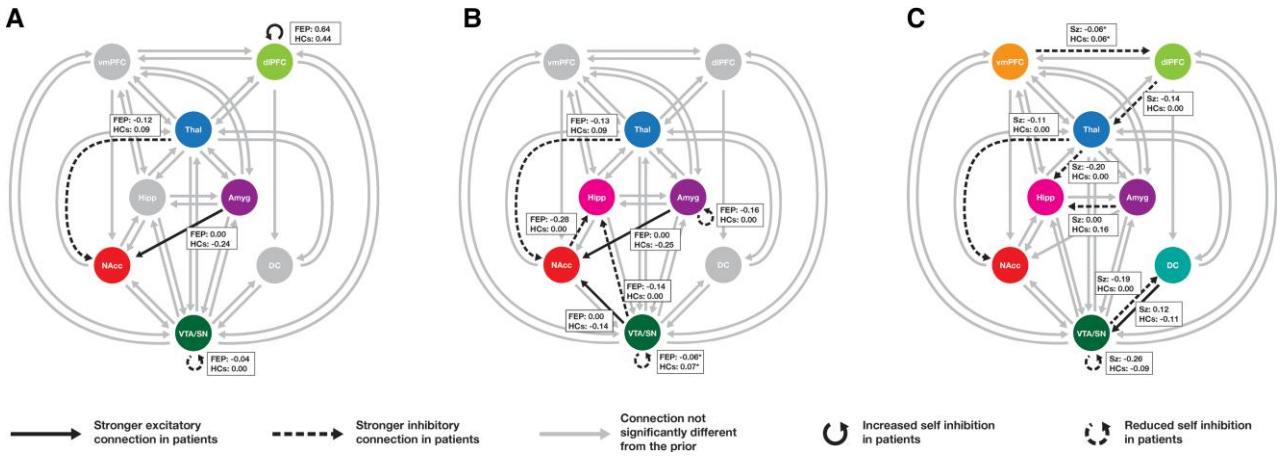


**Figure 2 Group differences in FST effective connectivity identified in FEP ($n = 46$), FEP-SCZ ($n = 17$), and SCZ ($n = 36$) patients relative to their respective control groups**. Differences in effective connectivity between FEP patients and healthy controls (HCs) are shown in **A**; the subgroup of FEP patients with schizophrenia-spectrum diagnosis are shown in **B**; and patients with established schizophrenia (Sz) and HCs are shown in **C**. Boxes show mean connectivity values in each group. For connections between regions, dashed arrows represent connections for which patients show an increased inhibitory influence compared to controls; solid arrows represent connections for which patients show increased excitatory influence compared with controls. For self-connections, dashed arrows represent reduced inhibition and solid arrows indicate increased inhibition in patients compared with controls. Grey arrows represent modelled connections that were not significantly different from the prior. Inter-regional connectivity parameters are in Hz. Self-connection values are in negative log scale. Connections were thresholded at $P > 0.95$, which represents strong evidence. *Connections for which the mean in each group has low posterior model probability, but in which differences between groups surpassed $P > 0.95$.

and Table 2). SCZ patients also showed increased inhibitory influence of vmPFC on dlPFC, of dlPFC on thalamus, and of thalamus and amygdala on hippocampus. FEP-SCZ patients and SCZ patients both showed altered bottom-up connectivity of the VTA/SN. In FEP-SCZ, these disruptions primarily affected the limbic circuit; in SCZ patients, they affected the dorsal system, with increased inhibitory influence on the DC on VTA/SN and an increased excitatory influence running in the reverse direction, from DC to VTA/SN.

## Associations with positive symptoms

Having identified both common and distinct disruptions of FST circuitry in FEP and SCZ patients, we next examined the association between specific FST connections (i.e. how much a region influences another) and psychotic symptom severity in both groups.

### First-episode psychosis

Greater positive symptom severity was predominantly associated with subcortical connectivity (Fig. 3A and Table 3). Specifically, more severe symptoms were associated with a relatively stronger influence of VTA/SN on NAcc and amygdala, and of NAcc and hippocampus on VTA/SN. More severe symptoms were also associated with a weaker influence of VTA/SN on DC and hippocampus, and with reduced self-inhibition of the amygdala. In cortex, higher positive symptom ratings were associated with weaker influence of dlPFC on vmPFC and weaker self-inhibition of vmPFC.

The FEP-SCZ subgroup (Fig. 3B and Table 3) showed similar associations with vmPFC self-inhibition and subcortical connectivity, although associations with hippocampal to VTA/SN connectivity and amygdala self-inhibition were absent. Positive symptom severity was additionally associated with a weaker influence of NAcc on hippocampus, of hippocampus on amygdala, of DC on thalamus, and reduced dlPFC self-inhibition, coupled with a stronger influence of dlPFC on thalamus and stronger thalamic self-inhibition.

### Established schizophrenia

Both cortical-subcortical and subcortical-cortical influences were associated with positive symptoms in SCZ patients (Fig. 3C and Table 3). Specifically, more severe positive symptoms were associated with a stronger top-down influence of vmPFC on VTA/SN and hippocampus; stronger bottom-up influence of VTA/SN on dlPFC; stronger influence of DC on thalamus and of thalamus on hippocampus; and greater dlPFC self-inhibition. Higher positive symptom ratings were also associated with weaker vmPFC and VTA/SN self-inhibition and a weaker influence of dlPFC on thalamus, thalamus on VTA/SN, VTA/SN on amygdala, hippocampus on vmPFC. Some common connections were implicated in both FEP-SCZ and SCZ patients (i.e. VTA/SN–amygdala, DC–thalamus, dlPFC–thalamus, and dlPFC self-inhibition), albeit with opposing polarity, suggesting that the link between positive symptoms and altered FST effective connectivity varies across illness stages.

## Associations with negative symptoms

Associations with negative symptom for FEP, FEP-SCZ, and SCZ patients are presented in Supplementary Fig. 2 and Supplementary Table 1. Associations between negative symptom severity and amygdala self-inhibition were consistent, albeit with reversed polarity, across the last two groups. Top-down cortical to subcortical connections were associated with negative symptom severity in FEP-SCZ patients, whereas SCZ patients showed associations with bottom-up subcortical to cortical connections. Similar to positive symptoms, negative symptom associations in FEP patients mainly implicated subcortical connections.

## Associations with striatal dopamine synthesis capacity

The analysis of clinical patients identified a prominent role for subcortical dysconnectivity in both FEP and SCZ groups. Dopamine

**Table 2 Summary of group differences in FST effective connectivity in FEP ($n = 46$), FEP–SCZ ($n = 17$), and SCZ ($n = 36$) patients respective to healthy controls**

| Connection | Increased (+) or decreased (–) in patients | Excitatory (E) or inhibitory (I) in patients | Effect size (Hz) | 90% posterior CI (lower bound, upper bound) | Patients (mean) | HC (mean) |
|---|---|---|---|---|---|---|
| **FEP versus HC** | | | | | | |
| *dlPFC → dlPFC* | + | *E* | 0.10 | 0.03, 0.20 | 0.64 | 0.44 |
| Thal → NAcc | – | I | 0.10 | –0.20, –0.01 | –0.12 | 0.09 |
| Amyg → NAcc | + | E | 0.11 | 0.02, 0.21 | 0.00 | –0.24 |
| *VTA/SN →* | – | *I* | 0.14 | –0.24, –0.04 | –0.04 | 0.00 |
| *VTA/SN* | | | | | *(–0.48)* | *(–0.05)* |
| **FEP–SCZ versus HC** | | | | | | |
| Thal → NAcc | – | I | 0.13 | –0.24, –0.03 | –0.13 | 0.09 |
| Amyg → NAcc | + | E | 0.13 | 0.02, 0.23 | 0.00 | –0.25 |
| *Amyg → Amyg* | – | *I* | *0.11* | *–0.22, 0.00* | *–0.16* | *0.00* |
| | | | | | *(–0.43)* | *(–0.05)* |
| NAcc → Hipp | – | I | 0.15 | –0.26, –0.04 | –0.28 | 0.00 |
| VTA/SN → Hipp | – | I | 0.09 | –0.20, –0.02 | –0.14 | 0.00 |
| VTA/SN → NAcc | + | E | 0.09 | –0.01, 0.20 | 0.00 | –0.14 |
| *VTA/SN →* | – | *I* | 0.08 | –0.19, 0.03 | –0.06[a] | 0.07[a] |
| *VTA/SN* | | | | | *(–0.47)* | *(–0.54)* |
| **SCZ versus HC** | | | | | | |
| dlPFC → Thal | – | I | 0.11 | –0.19, –0.03 | –0.14 | 0.00 |
| vmPFC → dlPFC | – | I | 0.08 | –0.16, 0.00 | –0.06[a] | 0.06[a] |
| Thal → Hipp | – | I | 0.10 | –0.18, –0.02 | –0.20 | 0.00 |
| Thal → NAcc | – | I | 0.09 | –0.17, –0.01 | –0.11 | 0.00 |
| Amyg → Hipp | – | E | 0.09 | –0.17, –0.01 | 0.00 | 0.16 |
| *VTA/SN →* | – | *I* | 0.16 | –0.25, –0.07 | *–0.26* | *–0.09* |
| *VTA/SN* | | | | | *(–0.39)* | *(–0.46)* |
| VTA/SN → DC | – | I | 0.14 | –0.22, –0.06 | –0.19 | 0.00 |
| DC → VTA/SN | + | E | 0.16 | 0.08, 0.25 | 0.12 | –0.11 |

Only connections surpassing a posterior probability threshold of 0.95 are presented in this table, and all reported connections have the posterior probability value of 1.00. All parameters for between region connections are in Hz. Self-connections are italicized, and values are log-transformed to ensure prior negativity (i.e. inhibitory) constraints on self-connections. A positive value for self-connection denotes increased inhibition; a negative value signifies reduced inhibition. Self-connection parameters in Hz are displayed in parentheses. Amyg = amygdala; CI = confidence interval; HC = healthy controls; Hipp = hippocampus; Thal = thalamus.

[a]Denotes connections for which the mean in each group has low posterior model probability, but in which differences between groups surpassed $P > 0.95$.

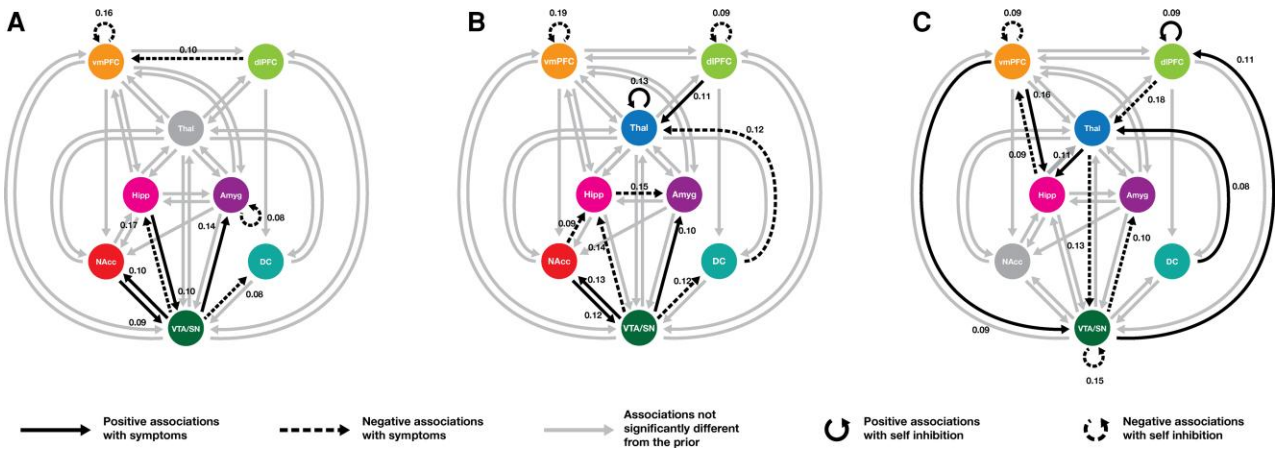


**Figure 3 Associations between positive symptoms and FST effective connectivity parameters in FEP ($n = 46$), FEP-SCZ ($n = 17$), and SCZ ($n = 36$) patients.** Panels from *left* to *right* depict the results of PEB models mapping associations between FST effective connectivity and positive symptoms in (**A**) FEP, (**B**) FEP-SCZ, and (**C**) SCZ patients. For between-region connections, solid arrows denote positive associations and dashed arrows depict negative associations between effective connectivity parameters and symptoms. For self-connections, solid arrows represent positive associations between symptom severity and self-inhibition, whereas dashed arrows denote negative associations such as more severe symptoms were associated with reduced inhibition. Grey arrows show modelled associations that were not (significantly) different from the prior. Connections were thresholded at $P > 0.95$. Amyg = amygdala; Hipp = hippocampus; Thal = thalamus.

**Table 3 Summary of connections associated with severity of positive symptoms in FEP ($n = 46$), FEP-SCZ ($n = 17$), and SCZ ($n = 36$) patients**

| Connection | Positive (+) or negative (–) association | Effect size (Hz) | 90% posterior CI (lower bound, upper bound) |
|---|---|---|---|
| **Positive symptoms** | | | |
| **FEP** | | | |
| dlPFC → vmPFC | – | 0.10 | –0.20, 0.01 |
| *vmPFC → vmPFC* | – | *0.16* | *–0.27, –0.06* |
| *Amyg → Amyg* | – | *0.08* | *–0.19, 0.02* |
| Hipp → VTA/SN | + | 0.10 | 0.00, 0.20 |
| NAcc → VTA/SN | + | 0.09 | –0.01, 0.20 |
| VTA/SN → NAcc | + | 0.09 | –0.02, 0.20 |
| VTA/SN → Hipp | – | 0.17 | –0.27, –0.06 |
| VTA/SN → Amyg | + | 0.14 | 0.04, 0.25 |
| VTA/SN → DC | – | 0.08 | –0.19, 0.02 |
| **FEP–SCZ** | | | |
| *vmPFC → vmPFC* | – | *0.19* | *–0.33, –0.05* |
| *dlPFC → dlPFC* | – | *0.09* | *–0.23, 0.04* |
| dlPFC → Thal | + | 0.11 | –0.02, 0.24 |
| *Thal → Thal* | + | *0.13* | *0.00, 0.26* |
| Hipp → Amyg | – | 0.15 | –0.28, –0.02 |
| NAcc → Hipp | – | 0.09 | –0.22, 0.03 |
| NAcc → VTA/SN | + | 0.12 | –0.01, 0.25 |
| DC → Thal | – | 0.12 | –0.25, 0.02 |
| VTA/SN → NAcc | + | 0.13 | 0.01, 0.26 |
| VTA/SN → Hipp | – | 0.14 | –0.27, –0.01 |
| VTA/SN → Amyg | + | 0.10 | –0.03, 0.23 |
| VTA/SN → DC | – | 0.12 | –0.25, 0.01 |
| **SCZ** | | | |
| *vmPFC → vmPFC* | – | *0.09* | *–0.20, 0.03* |
| vmPFC → Hipp | + | 0.16 | 0.05, 0.27 |
| vmPFC → VTA/SN | + | 0.08 | –0.03, 0.20 |
| *dlPFC → dlPFC* | + | *0.09* | *–0.03, 0.21* |
| dlPFC → Thal | – | 0.18 | –0.24, –0.06 |
| Thal → Hipp | + | 0.11 | 0.00, 0.22 |
| Tha → VTA/SN | – | 0.13 | –0.24, –0.02 |
| Hipp → vmPFC | – | 0.09 | –0.21, 0.02 |
| DC → Thal | + | 0.08 | –0.03, 0.19 |
| *VTA/SN → VTA/SN* | – | *0.15* | *–0.27, –0.04* |
| VTA/SN → Amyg | – | 0.10 | –0.21, 0.01 |
| VTA/SN → dlPFC | + | 0.11 | 0.00, 0.21 |

Only connections surpassing a posterior probability threshold of 0.95 are presented in this table, and all reported connections have the posterior probability value of 1.00.

All parameters for between region connections are in Hz. Self-connections are italicized, and values are log-transformed to ensure prior negativity (i.e. inhibitory) constraints on self-connections. A positive value for self-connection denotes increased inhibition, a negative value signifies reduced inhibition. Positive symptoms measured with BPRS positive subscale. Amyg = amygdala; CI = confidence interval; Hipp = hippocampus; Thal = thalamus.

dysregulation plays a central role in the genesis of psychotic symptoms[73–75] and there is robust evidence for elevated pre-synaptic dopamine synthesis capacity, as measured with $^{18}$F-DOPA, in the dorsal striatum of patients and at-risk individuals,[10,40,41] Dopaminergic transmission is influenced by, and influences, FST function.[8,9,76,77] We therefore set out to identify FST circuit elements that are associated with striatal $^{18}$F-DOPA in an independent sample of healthy individuals who underwent concurrent PET-fMRI.

### Dorsal striatum

Significant associations with dorsal striatal $^{18}$F-DOPA in healthy individuals largely implicated the thalamus (Fig. 4 and Table 4). Specifically, higher $^{18}$F-DOPA was associated with stronger thalamic self-inhibition; stronger thalamic influence over the VTA/SN and DC; stronger amygdala influence over thalamus; and a weaker influence of DC on thalamus. Stronger bottom-up influence of the amygdala on vmPFC was also associated with higher dorsal striatal $^{18}$F-DOPA.

### Ventral striatum

Ventral striatal $^{18}$F-DOPA was associated with a distributed set of extrinsic effective connections centered on midbrain and thalamus (Fig. 4 and Table 4). Specifically, higher $^{18}$F-DOPA was associated with weaker self-inhibition of NAcc and amygdala, a weaker influence of these two regions on the thalamus, and a stronger influence of hippocampus on thalamus. Ventral striatal $^{18}$F-DOPA was also associated with greater self-inhibition of the VTA/SN; weaker bottom-up influences of VTA/SN on the vmPFC and DC; weaker and stronger top-down influences of DC and hippocampus on VTA/SN, respectively; and greater DC self-inhibition.

## Discussion

FST dysfunction has been identified in psychotic illnesses,[2–5,16,18–20] but a characterization of how causal influences within these circuits are altered at distinct illness stages has been lacking. Using spectral DCM, we mapped the effective connectivity of dorsal and ventral FST circuits in FEP and established SCZ. Both clinical groups showed consistent disinhibition of VTA/SN and a stronger top-down inhibitory influence of the thalamus on NAcc. Altered top-down connectivity from the cortex to subcortex was only identified in established illness. Positive symptom severity was associated with a relative disinhibition of the VTA/SN in both illness stages. Additional associations were otherwise largely confined to subcortical connectivity in FEP and a distributed set of cortical and subcortical connections in SCZ patients. Concurrent PET-MRI in healthy individuals revealed distinct sets of FST connections associated with dorsal and ventral dopamine synthesis capacity, with DC and striatothalamic connectivity associated with both striatal dopamine synthesis and positive symptom severity. Our findings indicate that midbrain dysfunction and subcortical dysconnectivity is prominent in early illness stages, that cortical dysfunction becomes more salient in established illness, and that striatothalamic and nigrostriatal connectivity are related to both striatal dopamine synthesis capacity and positive symptom severity in patients.

### Effective dysconnectivity of fronto-striato-thalamic circuitry

We observed VTA/SN disinhibition across both illness stages, suggesting that it represents a core feature of FST pathology in psychosis. Midbrain disinhibition is consistent with elevated striatal dopamine synthesis.[10] Given that we found no evidence of disrupted top-down influences on VTA/SN in FEP in our modelled regions, our findings thus suggest that prior reports of elevated striatal dopamine in $^{18}$F-DOPA and other PET studies across different stages of psychosis may be linked to intrinsic dysregulation of the midbrain.[28,78]

Both FEP and SCZ groups also showed increased inhibitory influence of thalamus over NAcc. Excitatory thalamostriatal projections

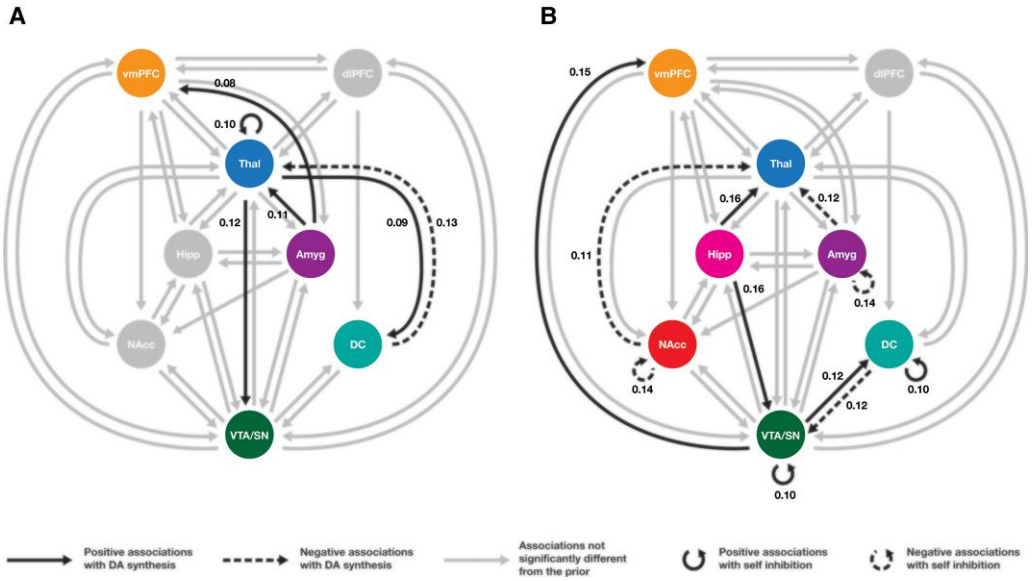


**Figure 4 Associations between FST connectivity and striatal dopamine synthesis capacity.** (**A**) Connections associated with dopamine synthesis in the dorsal circuit. (**B**) Associations with dopamine synthesis in the ventral circuit. Solid arrows: positive associations between effective connectivity parameters and dopamine synthesis; dashed arrows: negative associations between effective connectivity parameters and dopamine synthesis; grey arrows: modelled connections that were not (significantly) different from the prior. For self-connections, solid arrows represent positive associations between striatal dopamine synthesis and self-inhibition, whereas dashed arrows denote negative associations between striatal dopamine synthesis and self-inhibition. Connections were thresholded at $P > 0.95$. Amyg = amygdala; Hipp = hippocampus; Thal = thalamus.

provide feedback for the striatum to maintain bottom-up signalling to thalamus and cortex in support of specific actions or behaviours.[79] A greater inhibitory influence of thalamus on NAcc in both FEP and SCZ thus implies a dysregulation of the thalamostriatal feedback pathway. Although this dysregulation was not directly tied to VTA/SN function in our findings, animal models suggest that NAcc dysregulation can disinhibit the midbrain in young adult rats.[28,80] Notably, we have recently found that antipsychotics rapidly and preferentially impact thalamo-striatal and thalamo-cortical functional connectivity in FEP patients,[81] suggesting that a remediation of thalamic interactions with the rest of the brain may be a key therapeutic mechanism.

SCZ patients showed increased inhibitory influence of VTA/SN over DC, which may disrupt the capacity of this area to filter information through the FST circuits.[9,82] SCZ patients also showed increased top-down excitatory influence of DC over VTA/SN, which may reflect a compensatory response to regulate disinhibited signalling from the midbrain. Given that VTA/SN disinhibition was also observed in FEP, our findings suggest that an early bottom-up pathology of the midbrain may evolve to affect striatal function and potentially dysregulate feedback loops within the dorsal FST with illness progression. However, we cannot rule out an effect of medication in the SCZ group and longitudinal data are required to test this hypothesis.

In FEP, cortical dysfunction was limited to increased dlPFC self-inhibition. Post-mortem work has identified robust changes in GABAergic neuron function in patients with established schizophrenia,[83] but in vivo studies of FEP patients have been inconsistent, with reports of lower, higher, or no differences in prefrontal GABA levels.[32,33,84,85] Our findings thus suggest that while DLPFC dysfunction is evident early in psychosis, it does not to play a prominent role in broader FST dysfunction.

Taken together, our DCM analysis indicates that the early phase of psychosis is associated with prominent dysfunction of subcortical systems, with alterations in cortico-subcortical connectivity emerging in later illness stages. Intrinsic dysfunction of the VTA/SN and dlPFC, and altered thalamic regulation over the NAcc, appear to be stable features of the illness.

## Fronto-striato-thalamic connectivity and symptom severity

A primary role for VTA/SN dysregulation in psychosis is supported by our observations of consistent correlations between the connectivity of this region and positive symptom severity across illness stages.[26,86–88] However, the specific connections implicated varied across the patient groups. In the full FEP cohort, greater positive symptom severity was associated with connectivity between VTA/SN and limbic subcortical regions, which accords with a role for hippocampal–midbrain dysregulation identified in rodent models of psychosis.[28] Disinhibition of the vmPFC, another component of the limbic FST system, was negatively associated with positive symptom severity across the FEP, FEP-SCZ, and SCZ patients.[89,90]

Reduced influence of VTA/SN on DC was also associated with greater positive symptom severity in both FEP-SCZ and SCZ patients. When taken with evidence of robust [$^{18}$F]DOPA elevations in the DC in early psychosis,[10,11,41] our findings of intrinsic dysfunction of the midbrain across illness stages (see also Modinos *et al.*,[23] Howes *et al.*,[24] and Allen *et al.*[25]), and anatomical studies indicating that midbrain afferents to the dorsal striatum primarily originate in the SN,[8] our results identify a close link between nigrostriatal signalling and the expression of psychotic symptoms.

Several additional FST elements were consistently associated with positive symptom severity in both SCZ and FEP-SCZ patients, although the polarity of associations was often reversed between the FEP and SCZ groups. This reversal may be due to several factors,

**Table 4 Summary of connections associated with striatal dopamine synthesis**

| Connection | Positive (+) or negative (–) association | Effect size (Hz) | 90% posterior CI (lower bound, upper bound) |
|---|---|---|---|
| **Dorsal striatum** | | | |
| *Thal → Thal* | + | 0.10 | –0.04, 0.23 |
| Thal → DC | + | 0.09 | –0.04 0.22 |
| Thal → VTA/SN | + | 0.12 | –0.01, 0.26 |
| Amyg → vmPFC | + | 0.08 | –0.05, 0.21 |
| Amyg → Thal | + | 0.11 | –0.02, 0.24 |
| DC → Thal | – | 0.13 | –0.26, 0.00 |
| **Ventral striatum** | | | |
| Hipp → Thal | + | 0.16 | 0.03. 0.30 |
| Hipp → VTA/SN | + | 0.16 | 0.03, 0.29 |
| Amyg → Thal | – | 0.12 | –0.25, 0.02 |
| NAcc → Thal | – | 0.11 | –0.24, 0.02 |
| *Amyg → Amyg* | – | 0.14 | –0.27, 0.01 |
| *NAcc → NAcc* | – | 0.14 | –0.28, 0.00 |
| DC → VTA/SN | – | 0.12 | –0.25, 0.01 |
| *DC → DC* | + | 0.10 | –0.03, 0.22 |
| *VTA/SN → VTA/SN* | + | 0.10 | –0.05, 0.25 |
| VTA/SN → vmPFC | + | 0.15 | 0.02, 0.29 |
| VTA/SN → DC | + | 0.12 | –0.01, 0.25 |

Only connections surpassing a posterior probability threshold of 0.95 are presented in this table, and all reported connections have the posterior probability value of 1.00.

All parameters for between region connections are in Hz. Self-connections are italicized, and values are log-transformed to ensure prior negativity (i.e. inhibitory) constraints on self-connections. A positive value for self-connection denotes increased inhibition, a negative value signifies reduced inhibition. Amyg = amygdala; CI = confidence interval; Hipp = hippocampus; Thal = thalamus.

including differences in the neural correlates of psychotic symptoms at different illness stages, an effect of medication in the SCZ group, or a combination of both. Dopamine is proposed to regulate neuronal signalling in complex ways, and it is as yet unclear how dopamine levels at different illness stages relate to measures of functional or effective connectivity.[91,92] Precisely understanding these effects, and the impact of antipsychotic medication, is an important topic for further investigation.

There was less consistency across the cohorts with respect to negative symptom associations, with different sets of connections being associated with symptom severity in the FEP and SCZ groups. In general, the SCZ cohort demonstrated associations that were more widespread across the cortical and subcortical regions compared to the FEP and FEP-SCZ groups. Across both FEP and SCZ cohorts, the dlPFC and subcortical limbic regions, including the amygdala and the hippocampus, were generally implicated, consistent with evidence of prefrontal and limbic involvement in this symptom dimension.[93–95]

## Fronto-striato-thalamic connectivity and striatal dopamine synthesis capacity

Dorsal and ventral striatal $^{18}$F-DOPA levels were associated with effective connectivity of distinct FST circuit elements. Most associations with dorsal striatum $^{18}$F-DOPA were limited to the dorsal FST circuit and involved the thalamus. Two thalamic connections—an afferent input from DC and the thalamic self-connection—were also associated with positive symptom severity in FEP-SCZ patients. The modulation of cortical and thalamic glutamatergic signals by striatal dopamine controls striatothalamic filtering and information flow to the cortex, which is thought to play a central role in the pathogenesis of psychosis.[9] The close link between striatal $^{18}$F-DOPA and thalamic connectivity that we identify here may be related to evidence that antipsychotics preferentially impact thalamo-striatal and thalamo-cortical functional connectivity in FEP, and can recover FST connectivity following treatment.[81,96]

Bidirectional connectivity between the VTA/SN and DC was associated with dorsal striatal $^{18}$F-DOPA. This connection was identified as dysfunctional in SCZ patients and was correlated with positive symptom severity in both SCZ and FEP-SCZ. This consistency of findings suggests a close link between nigrostriatal signalling, striatal dopamine synthesis capacity, and positive symptom severity in patients. Notably, positive symptom severity in FEP was associated with a reduced influence of VTA/SN on DC, whereas higher dorsal striatal $^{18}$F-DOPA was associated with an increased afferent influence of VTA/SN. Since patients are known to show elevated $^{18}$F-DOPA in the dorsal striatum,[10,11] one might expect a negative association between striatal $^{18}$F-DOPA and VTA/SN-DC connectivity. One potential explanation is that elevated dopamine levels lead to compensatory changes in circuit function that affect the optimal balance of signalling between different regions, thus resulting in different circuit mechanisms that regulate dopamine levels in the brains of psychotic and non-psychotic individuals. Concurrent PET-fMRI in both patients and controls would help to test this possibility.

Connections associated with ventral striatal $^{18}$F-DOPA were distributed across the ventral and dorsal systems. NAcc projections are widely distributed in the midbrain and drive dorsal striatal dopamine levels.[8] Accordingly, we found that ventral striatal $^{18}$F-DOPA was associated with VTA/SN–DC connectivity and inhibition within both regions. VTA/SN–DC connectivity was also disrupted in SCZ patients and associated with positive symptoms in FEP, suggesting a link between the NAcc's regulation of midbrain activity and dorsal circuit dysfunction in patients.[97]

## Limitations and future directions

We used independent samples to cross-sectionally characterize effective dysconnectivity across distinct illness stages. This approach offers a test of consistency across cohorts, but inferences about the progression of circuit dysfunction must be confirmed longitudinally, especially given the differences in sample size and symptom severity across the three cohorts.

Psychosis is a highly heterogenous syndrome and diagnostic differences in our cohort may potentially complicate interpretation of our results. FST and dopamine dysfunction have been implicated in the onset of psychotic symptoms, regardless of the underlying diagnosis. In our past work, we have identified common disruptions of FST functional connectivity across people with FEP,[2] first episode mania with psychosis,[98] at-risk mental state with

psychosis,[3] and in association with high levels of subclinical schizotypy.[4,99] Given this evidence for transdiagnostic effects, and that first-episode diagnoses can sometimes be unstable,[100,101] it is critical to examine the FEP cohort as a group. The similarity in findings obtained with the full FEP and FEP-SCZ sub-groups with respect to subcortical and midbrain dysconnectivity and symptom associations indicate that diagnostic heterogeneity does not make a major contribution to our findings.

As the SCZ patients were medicated, the effects of antipsychotics on the brain should also be considered when interpreting the findings.[81] Although we did not find and significant associations between antipsychotic dose and effective connectivity parameters, only limited information on medication exposure was available for this open dataset;[43] therefore, further investigation of the specific effects of antipsychotic treatment on FST effective connectivity is warranted.

Our PEB analysis of the PET data identifies associations with, but not causal influences on, striatal $^{18}$F-DOPA. Further investigation of patients would be required to identify precisely how effective dysconnectivity of FST systems leads to dopamine dysregulation in patients. One interesting future avenue of work could use effective connectivity measures to develop multivariate predictive models of symptoms and dopamine synthesis capacity across different cohorts.

We restricted our analysis to left hemisphere FST ROIs previously implicated in past work as showing disrupted functional connectivity or as being key elements of FST circuitry.[2,3] This focus facilitates efficient estimation of DCMs but may miss influences from other key regions extending beyond the circuits studied here, such as the anterior cingulate cortex and anterior insula or even other areas of lateral PFC or thalamus. Recent improvements in the scalability of DCM[102] may be used to generate more anatomically comprehensive maps of effective dysconnectivity in psychosis.

## Conclusions

Our analysis characterized FST effective dysconnectivity in FEP and established schizophrenia. Our findings indicate that subcortical dysfunction features prominently in early illness stages, with cortical abnormalities becoming more apparent later in the illness. In early psychosis, positive symptoms are associated with midbrain connectivity, suggesting that aberrant bottom-up signals emanating from the midbrain may present a key FST feature in the pathogenesis of psychotic symptoms. In light of other findings strongly implicating cortical pathology in early illness stages,[103,104] our results suggest that this pathology may emerge after subcortical dysfunction, or that it may arise in cortical areas that were not modelled in our analysis. Nigrostriatal and striatothalamic connectivity are closely linked to striatal dopamine levels, while also being tied to symptom expression in patients. Together, our findings suggest a prominent role for subcortical systems in driving FST dysfunction in psychosis.

## Acknowledgements

We thank Drs Hannes Almgren and Ian Harding for advice on data analysis. The authors acknowledge the facilities and scientific and technical assistance of the National Imaging Facility, a National Collaborative Research Infrastructure Strategy (NCRIS) capability.

## Funding

This work was supported by the National Health and Medical Research Council (NHMRC) (ID: 1050504), Australian Research Council (ID: FT130100589) and the Charles and Sylvia Viertel Charitable Foundation. C.P. was supported by a NHMRC Senior Principal Research Fellowship (ID: 1105825). M.A-J. was supported by an Investigator Grant (APP1177235) from the National Health and Medical Research Council and a Dame Kate Campbell Fellowship from The University of Melbourne. V.C. was supported by a Brain & Behavior Research Foundation NARSAD Young Investigator Grant (21660).

## Competing interests

In the past 5 years, C.P. served on an advisory board for Lundbeck, Australia Pty Ltd. He has received honoraria for talks presented at educational meetings organized by Lundbeck. The other authors report no competing interests.

## Supplementary material

Supplementary material is available at *Brain* online.

## References

1. Haber SN. Corticostriatal circuitry. *Dialogues Clin Neurosci*. 2016;18(1):7–21.
2. Fornito A, Harrison BJ, Goodby E, *et al*. Functional dysconnectivity of corticostriatal circuitry as a risk phenotype for psychosis. *JAMA Psychiatry*. 2013;70(11):1143–1151.
3. Dandash O, Fornito A, Lee J, *et al*. Altered striatal functional connectivity in subjects with an at-risk mental state for psychosis. *Schizophr Bull*. 2014;40(4):904–913.
4. Sabaroedin K, Tiego J, Parkes L, *et al*. Functional connectivity of corticostriatal circuitry and psychosis-like experiences in the general community. *Biol Psychiatry*. 2019;86(1):16–24.
5. Anticevic A. Understanding the role of thalamic circuits in schizophrenia neuropathology. *Schizophr Res*. 2017;180:1–3.
6. Pantelis C, Barnes TR, Nelson HE, *et al*. Frontal-striatal cognitive deficits in patients with chronic schizophrenia. *Brain*. 1997;120:1823–1843.
7. Alexander GE, DeLong MR, Strick PL. Parallel organization of functionally segregated circuits linking basal ganglia and cortex. *Annu Rev Neurosci*. 1986;9:357–381.
8. Haber SN, Fudge JL, McFarland NR. Striatonigrostriatal pathways in primates form an ascending spiral from the shell to the dorsolateral striatum. *J Neurosci*. 2000;20(6):2369–2382.
9. Carlsson A, Waters N, Carlsson M. Neurotransmitter interactions in schizophrenia-therapeutic implications. *Biol Psychiatry*. 1999;46(10):1388–1395.
10. Howes OD, Bose S, Turkheimer F, *et al*. Progressive increase in striatal dopamine synthesis capacity as patients develop psychosis: a PET study. *Mol Psychiatry*. 2011;16(9):885–886.
11. Howes OD, Bose SK, Turkheimer F, *et al*. Dopamine synthesis capacity before onset of psychosis: A prospective [18F]-DOPA PET imaging study. *Am J Psychiatry*. 2011;11:1311–1317.
12. Kegeles LS, Abi-Dargham A, Frankle WG, *et al*. Increased synaptic dopamine function in associative regions of the striatum in schizophrenia. *Arch Gen Psychiatry*. 2010;67(3):231–239.
13. Mizrahi R, Addington J, Rusjan PM, *et al*. Increased stress-induced dopamine release in psychosis. *Biol Psychiatry*. 2012;71(6):561–567.

14. McGowan S, Lawrence AD, Sales T, Quested D, Grasby P. Presynaptic dopaminergic dysfunction in schizophrenia. *Arch Gen Psychiatry*. 2004;61(2):134.
15. Allen P, Chaddock CA, Howes OD, *et al*. Abnormal relationship between medial temporal lobe and subcortical dopamine function in people with an ultra high risk for psychosis. *Schizophr Bull*. 2012;38(5):1040–1049.
16. Horga G, Cassidy CM, Xu X, *et al*. Dopamine-related disruption of functional topography of striatal connections in unmedicated patients with schizophrenia. *JAMA Psychiatry*. 2016;73:862–870.
17. Woodward ND, Heckers S. Mapping thalamocortical functional connectivity in chronic and early stages of psychotic disorders. *Biol Psychiatry*. 2016;79(12):1016–1025.
18. Sarpal DK, Robinson DG, Fales C, *et al*. Relationship between duration of untreated psychosis and intrinsic corticostriatal connectivity in patients with early phase schizophrenia. *Neuropsychopharmacology*. 2017;42(11):2214–2221.
19. Wang Y, Ettinger U, Meindl T, Chan RCK. Association of schizotypy with striatocortical functional connectivity and its asymmetry in healthy adults. *Hum Brain Mapp*. 2018;39(1):288–299.
20. Kraguljac NV, White DM, Hadley N, *et al*. Aberrant hippocampal connectivity in unmedicated patients with schizophrenia and effects of antipsychotic medication: A longitudinal resting state functional mri study. *Schizophr Bull*. 2016;42(4):1046–1055.
21. Meyer-Lindenberg A, Miletich RS, Kohn PD, *et al*. Reduced prefrontal activity predicts exaggerated striatal dopaminergic function in schizophrenia. *Nat Neurosci*. 2002;5(3):267–271.
22. Fusar-Poli P, Howes OD, Allen P, *et al*. Abnormal prefrontal activation directly related to pre-synaptic striatal dopamine dysfunction in people at clinical high risk for psychosis. *Mol Psychiatry*. 2011;16(1):67–75.
23. Modinos G, Allen P, Grace AA, McGuire P. Translating the MAM model of psychosis to humans. *Trends Neurosci*. 2015;38(3):129–138.
24. Howes OD, Williams M, Ibrahim K, *et al*. Midbrain dopamine function in schizophrenia and depression: A post-mortem and positron emission tomographic imaging study. *Brain*. 2013;136(11):3242–3251.
25. Allen P, Luigjes J, Howes OD, *et al*. Transition to psychosis associated with prefrontal and subcortical dysfunction in ultra high-risk individuals. *Schizophr Bull*. 2012;38(6):1268–1276.
26. Hadley JA, Nenert R, Kraguljac NV, *et al*. Ventral tegmental area/midbrain functional connectivity and response to antipsychotic medication in schizophrenia. *Neuropsychopharmacology*. 2014;39(4):1020–1030.
27. Weinberger DR. Implications of normal brain development for the pathogenesis of schizophrenia. *Arch Gen Psychiatry*. 1987;44(7):660–669.
28. Lodge DJ, Grace AA. Aberrant hippocampal activity underlies the dopamine dysregulation in an animal model of schizophrenia. *J Neurosci*. 2007;27(42):11424–11430.
29. Dempster K, Jeon P, MacKinley M, Williamson P, Théberge J, Palaniyappan L. Early treatment response in first episode psychosis: a 7-T magnetic resonance spectroscopic study of glutathione and glutamate. *Mol Psychiatry*. 2020;25(8):1640–1650.
30. Merritt K, Egerton A, Kempton MJ, Taylor MJ, McGuire PK. Nature of glutamate alterations in schizophrenia a meta-analysis of proton magnetic resonance spectroscopy studies. *JAMA Psychiatry*. 2016;73(7):665–674.
31. Poels EMP, Kegeles LS, Kantrowitz JT, *et al*. Glutamatergic abnormalities in schizophrenia: A review of proton MRS findings. *Schizophr Res*. 2014;152(2–3):325–332.
32. Overbeek G, Gawne TJ, Reid MA, *et al*. Relationship between cortical excitation and inhibition and task-induced activation and deactivation: A combined magnetic resonance spectroscopy and functional magnetic resonance imaging study at 7T in first-episode psychosis. *Biol Psychiatry Cogn Neurosci Neuroimaging*. 2019;4(2):121–130.
33. de la Fuente-Sandoval C, Reyes-Madrigal F, Mao X, *et al*. Prefrontal and striatal gamma-aminobutyric acid levels and the effect of antipsychotic treatment in first-episode psychosis patients. *Biol Psychiatry*. 2018;83(6):475–483.
34. Reddy-Thootkur M, Kraguljac NV, Lahti AC. The role of glutamate and GABA in cognitive dysfunction in schizophrenia and mood disorders – A systematic review of magnetic resonance spectroscopy studies. *Schizophr Res*. 2020;24:S0920-9964(20)30077-3.
35. Egerton A, Modinos G, Ferrera D, McGuire P. Neuroimaging studies of GABA in schizophrenia: A systematic review with meta-analysis. *Transl Psychiatry*. 2017;7(6):e1147.
36. Friston KJ, Harrison L, Penny W. Dynamic causal modelling. *Neuroimage*. 2003;19(4):1273–1302.
37. Friston KJ. Functional and effective connectivity: A Review. *Brain Connect*. 2011;1(1):13–36.
38. Razi A, Kahan J, Rees G, Friston KJ. Construct validation of a DCM for resting state fMRI. *Neuroimage*. 2015;106:1–14.
39. Dandash O, Pantelis C, Fornito A. Dopamine, fronto-striato-thalamic circuits and risk for psychosis. *Schizophr Res*. 2017;180:48–57.
40. Egerton A, Chaddock CA, Winton-Brown TT, *et al*. Presynaptic striatal dopamine dysfunction in people at ultra-high risk for psychosis: Findings in a second cohort. *Biol Psychiatry*. 2013;74(2):106–112.
41. Howes OD, Montgomery AJ, Asselin MC, *et al*. Elevated striatal dopamine function linked to prodromal signs of schizophenia. *Arch Gen Psychiatry*. 2009;66(1):13–20.
42. Francey SM, O'Donoghue B, Nelson B, *et al*. Psychosocial intervention with or without antipsychotic medication for first-episode psychosis: A randomized noninferiority clinical trial. *Schizophr Bull Open*. 2020;1(1):1–11.
43. Poldrack RA, Congdon E, Triplett W, *et al*. A phenome-wide examination of neural and cognitive function. *Sci Data*. 2016;3:1–12.
44. Leucht S, Samara M, Heres S, Davis JM. Dose Equivalents for antipsychotic drugs: The DDD method. *Schizophr Bull*. 2016;42(1):S90–S94.
45. Dazzi F, Shafer A, Lauriola M. Meta-analysis of the brief psychiatric rating scale – expanded (BPRS-E) structure and arguments for a new version. *J Psychiatr Res*. 2016;81:140–151.
46. Esteban O, Markiewicz CJ, Blair RW, *et al*. fMRIPrep: a robust preprocessing pipeline for functional MRI. *Nat Methods*. 2019;16(1):111–116.
47. Treiber JM, White NS, Steed TC, *et al*. Characterization and correction of geometric distortions in 814 diffusion weighted images. *PLoS One*. 2016;11(3):e0152472
48. Parkes L, Fulcher BD, Yücel M, Fornito A. An evaluation of the efficacy, reliability, and sensitivity of motion correction strategies for resting-state functional MRI. *Neuroimage*. 2018;171:415–436.
49. Pruim RHR, Mennes M, van Rooij D, Llera A, Buitelaar JK, Beckmann CF. ICA-AROMA: A robust ICA-based strategy for removing motion artifacts from fMRI data. *Neuroimage*. 2015;112:267–277.
50. Friston KJ, Kahan J, Biswal B, Razi A. A DCM for resting state fMRI. *Neuroimage*. 2014;94(100):396–407.
51. Aquino KM, Fulcher BD, Parkes L, Sabaroedin K, Fornito A. Identifying and removing widespread signal deflections from

fMRI data: Rethinking the global signal regression problem. *Neuroimage*. 2020;212:116614.
52. Glasser MF, Coalson TS, Bijsterbosch JD, *et al*. Using temporal ICA to selectively remove global noise while preserving global signal in functional MRI data. *Neuroimage*. 2018;181: 692–717.
53. Hoffman JM, Meiega W, Hawk T, *et al*. The effectsof carbidopa administration on kinetics in positron emission tomography. *J Nucl Med*. 1992;33(8):1472–1477.
54. Ruottinen HM, Rinne JO, Ruotsalainen UH, *et al*. Striatal [18F] fluorodopa utilization after COMT inhibition with entacapone studied with PET in advanced Parkinson's disease. *J Neural Transm - Park Dis Dement Sect*. 1995;10(2–3):91–106.
55. Burgos N, Cardoso MJ, Thielemans K, *et al*. Attenuation correction synthesis for hybrid PET-MR scanners: Application to brain studies. *IEEE Trans Med Imaging*. 2014;33(12):2332–2341.
56. Baran J, Chen Z, Sforazzini F, *et al*. Accurate hybrid template-based and MR-based attenuation correction using UTE images for simultaneous PET/MR brain imaging applications. *BMC Med Imaging*. 2018;18(1):1–16.
57. Chen Z, Sforazzini F, Baran J, Close T, Shah NJ, Egan GF. MR-PET head motion correction based on co-registration of multicontrast MR images. *Hum Brain Mapp*. 2021;42:4081–4091.
58. Jenkinson M, Bannister P, Brady M, Smith S. Improved optimization for the robust and accurate linear registration and motion correction of brain images. *NeuroImage*. 2002;841:825–841.
59. Patlak CS, Blasberg RG. Graphical evaluation of blood-to-brain transfer constants from multiple-time uptake data. *J Cereb Blood Flow Metab*. 1985;5(4):584–590.
60. López-González FJ, Paredes-Pacheco J, Thurnhofer-Hemsi K, *et al*. QModeling: a multiplatform, easy-to-use and open-source toolbox for PET kinetic analysis. *Neuroinformatics*. 2019;17(1):103–114.
61. Parkes L, Fulcher BD, Yücel M, Fornito A. Transcriptional signatures of connectomic subregions of the human striatum. *Genes Brain Behav*. 2017;16(7):647–663.
62. Diedrichsen J, Balsters JH, Flavell J, Cussans E, Ramnani N. A probabilistic MR atlas of the human cerebellum. *Neuroimage*. 2009;46(1):39–46.
63. Dandash O, Harrison BJ, Adapa R, *et al*. Selective augmentation of striatal functional connectivity following NMDA receptor antagonism: Implications for psychosis. *Neuropsychopharmacology*. 2014;40(3):1–10.
64. Di Martino A, Scheres A, Margulies DS, *et al*. Functional connectivity of human striatum: A resting state fMRI study. *Cereb Cortex*. 2008;18(12):2735–2747.
65. Postuma RB, Dagher A. Basal ganglia functional connectivity based on a meta-analysis of 126 positron emission tomography and functional magnetic resonance imaging publications. *Cereb Cortex*. 2006;16(10):1508–1521.
66. Fischl B, Salat DH, Busa E, *et al*. Whole brain segmentation: neurotechnique automated labeling of neuroanatomical structures in the human brain. *Neuron*. 2002;33:341–355.
67. Small SA, Schobel SA, Buxton RB, Witter MP. A pathophysiological framework of hippocampal dysfunction in ageing and disease. *Nat Rev Neurosci*. 2011;12(10):585–601.
68. Zeidman P, Maguire EA. Anterior hippocampus: the anatomy of perception, imagination and episodic memory. *Nat Rev Neurosci*. 2017;17(3):173–182.
69. Murty VP, Shermohammed M, Smith DV, Carter RMK, Huettel SA, Adcock RA. Resting state networks distinguish human ventral tegmental area from substantia nigra. *Neuroimage*. 2014;100:580–589.
70. Friston KJ, Litvak V, Oswal A, *et al*. Bayesian model reduction and empirical Bayes for group (DCM) studies. *Neuroimage*. 2016;128:413–431.
71. Power JD, Barnes KA, Snyder AZ, Schlaggar BL, Petersen SE. Spurious but systematic correlations in functional connectivity MRI networks arise from subject motion. *Neuroimage*. 2012;59(3):2142–2154.
72. Zeidman P, Jafarian A, Corbin N, *et al*. A guide to group effective connectivity analysis, part 1: First level analysis with DCM for fMRI. *Neuroimage*. 2019;200:174–190.
73. Kapur S. Psychosis as a state of aberrant salience: a framework linking biology, phenomenology, and pharmacology in schizophrenia. *Am J Psychiatry*. 2003;160(1):13–23.
74. McCutcheon RA, Krystal JH, Howes OD. Dopamine and glutamate in schizophrenia: biology, symptoms and treatment. *World Psychiatry*. 2020;19(1):15–33.
75. Howes OD, Kapur S. The dopamine hypothesis of schizophrenia: Version III - The final common pathway. *Schizophr Bull*. 2009;35(3):549–562.
76. Grace AA. Dysregulation of the dopamine system in the pathophysiology of schizophrenia and depression. *Nat Rev Neurosci*. 2016;17(8):524–532.
77. Maia TV, Frank MJ. An integrative perspective on the role of dopamine in schizophrenia. *Biol Psychiatry*. 2017;81(1):52–66.
78. McCutcheon RA, Abi-Dargham A, Schizophrenia HO. Dopamine and the striatum: From biology to symptoms. *Trends Neurosci*. 2019;42(3):205–220.
79. Haber SN, McFarland NR. The place of the thalamus in frontal cortical-basal ganglia circuits. *Neuroscientist*. 2001;7(4):315–324.
80. Lodge DJ, Grace AA. Hippocampal dysregulation of dopamine system function and the pathophysiology of schizophrenia. *Trends Pharmacol Sci*. 2011;32(9):507–513.
81. Chopra S, Francey SM, O'Donoghue B, *et al*. Functional connectivity in antipsychotic-treated and antipsychotic-naive patients with first-episode psychosis and low risk of self-harm or aggression: A secondary analysis of a randomized clinical trial. *JAMA Psychiatry*. 2021;78(9):994–1004.
82. Carlsson M, Carlsson A. Interactions between glutamatergic and monoaminergic systems within the basal ganglia-implications for schizophrenia and Parkinson's disease. *Trends Neurosci*. 1990;13(7):272–276.
83. Lewis DA, Hashimoto T, Volk DW. Cortical inhibitory neurons and schizophrenia. *Nat Rev Neurosci*. 2005;6(4):312–324.
84. Wang AM, Pradhan S, Coughlin JM, *et al*. Assessing brain metabolism with 7-T proton magnetic resonance spectroscopy in patients with first-episode psychosis. *JAMA Psychiatry*. 2019;76(3):314–323.
85. Reid MA, Salibi N, White DM, Gawne TJ, Denney TS, Lahti AC. 7T proton magnetic resonance spectroscopy of the anterior cingulate cortex in first-episode schizophrenia. *Schizophr Bull*. 2019;45(1):180–189.
86. Sonnenschein SF, Gomes FV, Grace AA. Dysregulation of midbrain dopamine system and the pathophysiology of schizophrenia. *Front Psychiatry*. 2020;11:613.
87. Gradin VB, Waiter G, O'Connor A, *et al*. Salience network-midbrain dysconnectivity and blunted reward signals in schizophrenia. *Psychiatry Res – Neuroimaging*. 2013;211(2):104–111.
88. Winton-Brown TT, Schmidt A, Roiser JP, *et al*. Altered activation and connectivity in a hippocampal-basal ganglia-midbrain circuit during salience processing in subjects at ultra high risk for psychosis. *Transl Psychiatry*. 2017;7(10): e1245.

89. Taylor SF, Welsh RC, Chen AC, Velander AJ, Liberzon I. Medial frontal hyperactivity in reality distortion. *Biol Psychiatry*. 2007; 61(10):1171–1178.
90. Pankow A, Katthagen T, Diner S, *et al*. Aberrant salience is related to dysfunctional self-referential processing in psychosis. *Schizophr Bull*. 2016;42(1):67–76.
91. Conio B, Martino M, Magioncalda P, *et al*. Opposite effects of dopamine and serotonin on resting-state networks: review and implications for psychiatric disorders. *Mol Psychiatry*. 2020;25(1):82–93.
92. Cole DM, Beckmann CF, Oei NYL, Both S, van Gerven JMA, Rombouts SARB. Differential and distributed effects of dopamine neuromodulations on resting-state network connectivity. *Neuroimage*. 2013;78:59–67.
93. Makowski C, Bodnar M, Shenker JJ, *et al*. Linking persistent negative symptoms to amygdala–hippocampus structure in first-episode psychosis. *Transl Psychiatry*. 2017; 7(8):e1195.
94. Rajarethinam R, DeQuardo JR, Miedler J, *et al*. Hippocampus and amygdala in schizophrenia: Assessment of the relationship of neuroanatomy to psychopathology. *Psychiatry Res – Neuroimaging*. 2001;108(2):79–87.
95. Walton E, Hibar DP, Van Erp TGM, *et al*. Prefrontal cortical thinning links to negative symptoms in schizophrenia via the ENIGMA consortium. *Psychol Med*. 2018;48(1):82–94.
96. Sarpal DK, Robinson DG, Lencz T, *et al*. Antipsychotic treatment and functional connectivity of the striatum in first-episode schizophrenia. *JAMA Psychiatry*. 2015;72(1):5–13.
97. Lodge DJ, Grace AA. Divergent activation of ventromedial and ventrolateral dopamine systems in animal models of amphetamine sensitization and schizophrenia. *Int J Neuropsychopharmacol*. 2012;15(1):69–76.
98. Dandash O, Yücel M, Daglas R, *et al*. Differential effect of quetiapine and lithium on functional connectivity of the striatum in first episode mania. *Transl Psychiatry*. 2018;8(1):59.
99. Pani SM, Sabaroedin K, Tiego J, Bellgrove MA, Fornito A. A multivariate analysis of the association between corticostriatal functional connectivity and psychosis-like experiences in the general community. *Psychiatry Res – Neuroimaging*. 2021; 307:111202.
100. Addington J, Chaves A, Addington D. Diagnostic stability over one year in first-episode psychosis. *Schizophr Res*. 2006;86(1–3):71–75.
101. Whitty P, Clark M, McTigue O, *et al*. Diagnostic stability four years after a first episode of psychosis. *Psychiatr Serv*. 2005; 56(9):1084–1088.
102. Frässle S, Harrison SJ, Heinzle J, *et al*. Regression dynamic causal modeling for resting-state fMRI. *Hum Brain Mapp*. 2021;42: 2159–2180.
103. Seidman LJ, Thermenos HW, Poldrack RA, *et al*. Altered brain activation in dorsolateral prefrontal cortex in adolescents and young adults at genetic risk for schizophrenia: An fMRI study of working memory. *Schizophr Res*. 2006;85(1–3):58–72.
104. Sun D, Phillips L, Velakoulis D, *et al*. Progressive brain structural changes mapped as psychosis develops in “at risk” individuals. *Schizophr Res*. 2009;108(1–3):85–92.